Journal of Solid State Chemistry **143,** 246–253 (1999)
Article ID jssc.1998.8101, available online at http://www.idealibrary.com on IDEAL®

Hydrothermal Synthesis and Characterization of $M_2Te_3O_8$ (M = Mn, Co, Ni, Cu, Zn): A Series of Compounds with the Spiroffite Structure

Christopher R. Feger, George L. Schimek, and Joseph W. Kolis

Department of Chemistry, Clemson University, Clemson, South Carolina 29634

Received March 9, 1998; in revised form November 10, 1998; accepted November 22, 1998

Several compounds isotypic to the mineral spiroffite were obtained as high quality single crystals via hydrothermal reactions. These materials, which have the general formula $M_2Te_3O_8$, crystallize in the monoclinic space group $C2/c$ and contain divalent transition metal ions and tellurite building blocks. Typical synthetic conditions for the preparation of these materials are 375°C for 3–5 days in an aqueous NH_4Cl solution. This structure type is based on slabs containing Te_2O_6 groups joined by M cations. These Te_2O_6 groups are made up of two edge-sharing TeO_{3+1} polyhedra. The metal tellurite slabs are connected to one another through tellurium(IV) atoms, which are coordinated by four oxygen atoms in a regular TeO_4 trigonal bipyramidal configuration. A detailed structural characterization via single crystal X-ray diffraction was performed on four compounds ($Co_2Te_3O_8$: $a = 12.690(1)$ Å, $b = 5.211(2)$ Å, $c = 11.632(2)$ Å, $\beta = 98.98(1)°$, $V = 759.7(3)$ Å^3, $R(R_w) = 0.023$ (0.046); $Ni_2Te_3O_8$: $a = 12.407(1)$ Å, $b = 5.207(1)$ Å, $c = 11.509(1)$ Å, $\beta = 98.723(9)°$, $V = 735.0(2)$ Å^3, $R(R_w) = 0.025$ (0.033); $Cu_2Te_3O_8$: $a = 11.8368(8)$ Å, $b = 5.266(2)$ Å, $c = 12.2419(8)$ Å, $\beta = 100.316(6)°$, $V = 750.7(2)$ Å^3, $R(R_w) = 0.025$ (0.032); $Zn_2Te_3O_8$: $a = 12.681(2)$ Å, $b = 5.200(2)$ Å, $c = 11.786(2)$ Å, $\beta = 99.60(1)°$, $V = 766.3(3)$ Å^3, $R(R_w) = 0.031$ (0.041)). The manganese analog ($a = 12.896(5)$ Å, $b = 5.398(2)$ Å, $c = 11.907(5)$ Å, $\beta = 98.14(4)°$) was identified via powder diffraction patterns. The cobalt, nickel, and copper compounds were observed to have an antiferromagnetic transition by DC magnetic susceptibility measurements. The band gaps were obtained by optical diffuse reflectance spectroscopy and show that these compounds are all wide band gap materials.

INTRODUCTION

Tellurium(IV) oxides often adopt unusual structures based on uncommon main group coordination environments that arise due to the presence of a stereochemical lone pair. These compounds are also interesting from a fundamental viewpoint, as they provide insights into the structure of corresponding tellurite glasses. Tellurite glasses are desirable materials as they have high refractive indices (1), high infrared transmittance (2), and high electrical and ionic conductivities (3,4), as well as being resistant to devitrification. The study of ternary tellurites is necessary as TeO_2 is only a conditional glass former, forming stable glass systems only in the presence of network modifying cations (1).

Recently we have shown by using hydrothermal techniques that it is possible to obtain interesting new materials based on tellurite and tellurate building blocks in supercritical H_2O. These compounds, which include $Na_3Mn_4Te_2O_{12}$ (5), a material that crystallizes from alkaline solutions in a variant of the calcium ferrite structure, based on TeO_6 octahedra, and $Ba_2Cu_4Te_4O_{11}Cl_4$ and $BaCu_2Te_2O_6Cl_2$ (6), two compounds that are made up of TeO_3 and TeO_{3+1} units and can only be obtained from hydrothermal NH_4Cl solutions. These two units, TeO_3 and TeO_{3+1}, are common motifs in tetravalent tellurium oxide chemistry, with the TeO_3^{2-} fragment previously observed in several compounds such as $CuTe_2O_5$ (7), $CuTeO_3$ (8), and $NiTe_2O_5$ (9), and the TeO_{3+1}^{4-} fragment observed in $CuTe_2O_5$ (7), $Te_6O_{11}Cl_2$ (10), and V_2MnTeO_7 (11). In addition to these two fragments, tellurium also adopts a TeO_4^{2-} unit with C_{2v} symmetry which is best seen in α-TeO_2 (12).

During our studies on tellurate and tellurite materials, we isolated the material $Cu_2Te_3O_8$ which is isostructural to the mineral spiroffite, $(Mn, Zn)_2Te_3O_8$ (13). This mineral structure type was not fully structurally characterized until 1966 when Hanke reported the crystal structure of $Zn_2Te_3O_8$ (14). There have also been very brief and inconclusive reports of powder data on $Co_2Te_3O_8$ (15), $Ni_2Te_3O_8$ (16), and $Mn_2Te_3O_8$ (17), but no detailed structural information on these compounds could be found in our literature search. In this paper, we have obtained moderate to excellent yields of high quality single crystals of several members of the spiroffite family using hydrothermal methods. We have performed detailed crystallographic studies and obtained magnetic measurements and optical diffuse reflectance spectra of the cobalt, nickel, and copper analogs.

0022-4596/99 $30.00

EXPERIMENTAL

Synthesis

The compounds obtained in this study were prepared using modifications of techniques reported by Rabenau (18). All reactions were performed by loading the starting materials into fused silica tubing (5 mm id, 7 mm od, $\sim 1.6\ cm^3$ sealed volume). A 1 *M* NH_4Cl (0.7 mL, 45% fill) solution was added and the tubes were flame sealed after freezing the solvent in liquid nitrogen. After sealing, the tubes were placed in a high pressure autoclave which was pressurized to ~ 2500 psi of argon to prevent the explosion of the reaction tubes during heating. The autoclave was placed in a tube furnace and heated at 375°C for 3–5 days, after which the autoclave was removed directly from the furnace and allowed to cool. Starting materials used as received were CuO (Strem, 99.999%), ZnO (Strem, 99.7%), Mn_2O_3 (Strem, 99%), TeO_2 (Strem, 99 + %), and $Te(OH)_6$ (Strem, 99.5%). Co_3O_4 and NiO were obtained by the thermal decomposition of $CoCO_3$ (Strem, 99%) and $NiCO_3$ (Allied, 99%), respectively, at 900°C for 24 h.

$Cu_2Te_3O_8$ was obtained either by reacting 59 mg (0.74 mmol) of CuO and 170 mg (0.740 mmol) $Te(OH)_6$ with 22 mg (0.38 mmol) of NaCl or in a reaction of 48 mg (0.60 mmol) of CuO and 138 mg (0.601 mmol) of $Te(OH)_6$ with 73 mg (0.35 mmol) of $BaCl_2$ in a 1 *M* NH_4Cl solution. In both cases, the desired product was obtained as yellow, plate-like crystals in approximately 25% yield. When NaCl was used as the mineralizer, the bulk of remaining products was $CuTeO_4$ (yellow powder) (19), but when $BaCl_2$ was used the side products were $CuTeO_4$ and platy green crystals of $Ba_2Cu_4Te_4O_{11}Cl_4$ (6).

Both $Zn_2Te_3O_8$ (clear prisms) and $Ni_2Te_3O_8$ (yellow plates) were obtained in essentially quantitative yield when stoichiometric ratios of ZnO (51 mg, 0.63 mmol) or NiO (48 mg, 0.64 mmol) and TeO_2 (Zn reaction, 149 mg, 0.934 mmol; Ni reaction, 152 mg, 0.952 mmol) were reacted in 1 *M* NH_4Cl solution. In the nickel reaction, there were no detectable impurities by X-ray powder diffraction, and in the zinc reaction, there was only a small amount of $ZnTeO_3$ present.

$Co_2Te_3O_8$ was obtained in approximately 60% yield as purple polyhedra in a reaction containing 51 mg (0.21 mmol) of Co_3O_4 and 152 mg (0.952 mmol) of TeO_2 in a 1 M NH_4Cl solution. Byproducts in this reaction consisted largely of $CoTeO_4$ (brown powder) (20) and highly faceted, clear crystals of TeO_2. Yellow-brown prisms of $Mn_2Te_3O_8$ were obtained in approximately 75% yield from a reaction of Mn_2O_3 (51 mg, 0.32 mmol) and TeO_2 (154 mg, 0.965 mmol) in 1 *M* NH_4Cl solution. This product was accompanied by the known double oxides, $MnTe_6O_{13}$ (17) and Mn_3TeO_6 (21). Single crystal X-ray determinations were attempted on several crystals of $Mn_2Te_3O_8$, but all crystallites proved to be polycrystalline as determined by rotation photographs.

Crystallography

Suitable single crystals were mounted onto the ends of glass fibers using quick-drying epoxy and were studied on a Rigaku AFC7R four circle diffractometer equipped with graphite monochromated Mo$K\alpha$ ($\lambda = 0.71073$ Å) radiation. An ω-2θ scan was utilized for room temperature data collection. Three standard reflections measured after every 100 reflections indicated that all compounds were stable. A two-theta limit of 55° for data collection was employed for all materials. The intensity data were corrected for both Lorentz and polarization effects. Further details are included in Table 1.

The structure of $Cu_2Te_3O_8$ was determined first. The systematic absences hkl, $h + k = 2n + 1$ and $h0l$, $h, l = 2n + 1$ indicated that the space group could be either Cc or $C2/c$. The centrosymmetric space group, $C2/c$, was chosen based on statistical tests and subsequent successful refinement. The positions of the metal atoms were obtained by direct methods in the TEXSAN package (22) and the oxygen atoms were found during successive Fourier syntheses. The final structure was refined on $|F|$ by full, matrix least-squares techniques in SHELXTL-Plus (23). After absorption effects were compensated for by the use of empirical ψ-scan data (24) and an extinction parameter was applied (25), all atomic parameters were refined anisotropically. No higher symmetry was detected by the MISSYM algorithm within the PLATON program suite (26, 27). The structures of the remaining three compounds were refined in similar fashion by starting with the final positional parameters for $Cu_2Te_3O_8$. Crystallographic details for the structure determinations are given in Table 1. The final positional parameters and isotropic displacement coefficients for all compounds are given in Table 2. Relevant interatomic distances and angles are tabulated in Table 3.

Powder diffraction data were obtained using a Scintag XDS 2000 θ/θ diffractometer equipped with monochromated Cu$K\alpha$ radiation ($\lambda = 1.54056$ Å). The lattice parameters were obtained using a minimum of 25 lines from $2\theta = 5$–65°, based on an external quartz standard.

Physical Characterization

The magnetic susceptibility data were collected at Rice University using a Quantum Design SQUID magnetometer. Typical samples were ~ 20 mg of ground crystals which were placed in a gelatin pill capsule that was then held in a standard plastic drinking straw. Data were collected in a 1 *T* field from 5 to 300 K. The sample holder showed negligible diamagnetic effects on the bulk sample. Room temperature diffuse reflectance measurements from

TABLE 1
X-Ray Crystallographic Data

Compound	$Co_2Te_3O_8$	$Ni_2Te_3O_8$	$Cu_2Te_3O_8$	$Zn_2Te_3O_8$
Color, habit	purple plate	yellow rod	yellow parallelepiped	clear prism
Cryst size, mm^3	$0.02 \times 0.13 \times 0.13$	$0.07 \times 0.07 \times 0.17$	$0.02 \times 0.04 \times 0.07$	$0.17 \times 0.22 \times 0.24$
Space group	$C2/c$	$C2/c$	$C2/c$	$C2/c$
a (Å)	12.690(1)	12.407(1)	11.8368(8)	12.681(2)
b (Å)	5.211(2)	5.207(1)	5.266(2)	5.200(2)
c (Å)	11.632(2)	11.509(1)	12.2419(8)	11.786(2)
β (deg)	98.98(1)	98.723(9)	100.316(6)	99.60(1)
V ($Å^3$)	759.7(3)	735.0(2)	750.7(2)	766.3(3)
Z	4	4	4	4
Formula weight (g/mol)	628.66	628.20	637.89	641.56
D_{calc} (g/cm^3)	5.496	5.676	5.643	5.560
μ (cm^{-1})	156.73	168.07	171.65	174.68
F (000)	1096	1104	1112	1120
2θ range (°)	3.5–55.0	3.5–55.0	3.5–55.0	3.5–55.0
Scan type	$\omega/2\theta$	$\omega/2\theta$	$\omega/2\theta$	$\omega/2\theta$
Total reflns.	1005	983	1008	1022
Ind. reflns.	865	846	866	876
Ind. reflns. ($F_o > 4\sigma(F_o)$)	819	799	778	863
Refined parameters	61	61	61	61
Transmission factors	0.321–1.000	0.618–1.000	0.617–1.000	0.612–1.000
Extinction parameter	0.00057(5)	0.00116(8)	0.00185(8)	0.00115(5)
R^a, wR^b ($F_o > 4\sigma(F_o)$)	0.023, 0.046	0.025, 0.054	0.025, 0.033	0.036, 0.076
R^a, wR^b (all data)	0.025, 0.046	0.026, 0.055	0.029, 0.034	0.036, 0.076
S^c ($F_o > 4\sigma(F_o)$)	1.71	2.00	1.12	3.13
Max/min diff. peak ($e/Å^3$)	0.90/−1.11	1.73/−1.51	1.38/−1.22	1.96/−2.76
Max/mean shift	0.001/0.000	0.001/0.000	0.002/0.001	0.001/0.000

[a] $R = \sum||F_o| - |F_c||/\sum|F_o|$.
[b] $wR = [\sum w\{|F_o| - |F_c|\}^2/\sum w|F_o|^2]^{1/2}$; $w = 1/[\sigma^2\{|F_o|\} + 0.0005\{|F_o|^2\}]$.
[c] $S = [\sum w\{|F_o| - |F_c|\}^2/\{N_o - N_v\}]^{1/2}$; $w = 1/[\sigma^2\{|F_o|\} + 0.0005\{|F_o|^2\}]$; N_o, number of observations; N_v, number of variables.

2500 to 200 nm on the $Co_2Te_3O_8$, $Ni_2Te_3O_8$, and $Cu_2Te_3O_8$ were made using a Shimadzu UV3100 spectrophotometer equipped with an integrating sphere attachment. Barium sulfate was used as the reflectance standard. The reflectance data was converted to absorbance data using the Kubelka–Munk function (28).

RESULTS AND DISCUSSION

Synthesis

It was found that a wide variety of divalent first row transition metals will form the spiroffite structure. In attempts to synthesize an iron analog of the $M_2Te_3O_8$ series, the mineral phase rodalquilarite $H_3Fe_2(TeO_3)_4Cl$ (29), as determined by both powder and single crystal X-ray diffraction, was produced in high yield and quality. In our review of the literature, it became apparent that there was some confusion concerning a phase identified as the triclinic form of $Fe_2Te_4O_{11}$ (30) and this is discussed more fully in an accompanying paper (31).

In addition to the NH_4Cl mineralizer used to obtain the compounds in this study, a variety of other mineralizers were attempted. Several other chlorides, such as NaCl, KCl, $SrCl_2$, and $BaCl_2$ were used but failed to yield crystalline products. In most cases, the products were either amorphous or crystalline Te^{6+} products, such as $CoTeO_4$ and $CuTeO_4$. Additionally, mixtures of mineralizers were also attempted in efforts to obtain crystalline products. However, only mixtures that included NH_4Cl yielded desired products.

Attempts to use highly acidic solutions such as 0.1–1.0 *M* HCl solutions did not yield desired double oxides. In these cases, the metal oxide was completely converted to the chloride and the Te^{4+} in TeO_2 fully reduced to Te^0 presumably in the following reaction:

$$2\ MO(s) + 3\ TeO_2(s) \xrightarrow{HCL\ (xs)} 2\ M^{2+}(aq) + 2\ Cl^-(aq) + 3\ Te^0(s) + 3\ O_2\uparrow + 2\ H_2O \qquad [1]$$

The above equation is endothermic by 0.700 eV at 25°C in 1 *M* HCl (32). However, it is well known that reduction potentials tend to decrease dramatically at higher

TABLE 2
Atomic Coordinates and Equivalent Isotropic Thermal Parameters (Å²)

	X	*Y*	*Z*	U_{eq}[a]
		$Co_2Te_3O_8$		
Co	0.27021(7)	0.3024(1)	0.14805(7)	0.0096(3)
Te(1)	$\frac{1}{2}$	0.6541(1)	$\frac{1}{4}$	0.0095(2)
Te(2)	0.36416(3)	0.30911(7)	0.44390(3)	0.0091(2)
O(1)	0.4210(3)	0.4295(9)	0.1445(3)	0.015(1)
O(2)	0.3859(3)	0.6246(8)	0.3617(3)	0.012(1)
O(3)	0.3026(3)	0.1346(8)	0.3091(3)	0.012(1)
O(4)	0.2382(3)	0.4888(7)	0.4707(3)	0.010(1)
		$Ni_2Te_3O_8$		
Ni	0.26516(8)	0.3204(1)	0.14426(7)	0.0067(3)
Te(1)	$\frac{1}{2}$	0.6778(1)	$\frac{1}{4}$	0.0072(2)
Te(2)	0.36471(4)	0.31808(8)	0.44214(4)	0.0067(2)
O(1)	0.4185(4)	0.449(1)	0.1461(4)	0.013(1)
O(2)	0.3865(4)	0.6487(8)	0.3675(4)	0.009(1)
O(3)	0.2990(4)	0.1572(8)	0.3029(4)	0.009(1)
O(4)	0.2340(4)	0.4905(8)	0.4730(4)	0.008(1)
		$Cu_2Te_3O_8$		
Cu	0.26723(7)	0.2701(1)	0.15583(1)	0.0109(3)
Te(1)	$\frac{1}{2}$	0.6321(1)	$\frac{1}{4}$	0.0089(2)
Te(2)	0.36589(4)	0.28977(9)	0.44539(3)	0.0089(2)
O(1)	0.4152(4)	0.408(1)	0.1479(4)	0.015(1)
O(2)	0.3815(4)	0.5986(9)	0.3570(4)	0.012(1)
O(3)	0.3102(4)	0.0984(9)	0.3194(4)	0.013(1)
O(4)	0.2252(4)	0.4648(9)	0.4562(4)	0.010(1)
		$Zn_2Te_3O_8$		
Zn	0.27203(8)	0.2886(2)	0.15483(8)	0.0085(3)
Te(1)	$\frac{1}{2}$	0.6386(2)	$\frac{1}{4}$	0.0069(2)
Te(2)	0.36329(4)	0.3026(1)	0.44556(4)	0.0068(2)
O(1)	0.4206(5)	0.412(2)	0.1451(5)	0.019(2)
O(2)	0.3872(4)	0.612(1)	0.3610(4)	0.008(2)
O(3)	0.3038(5)	0.125(1)	0.3127(4)	0.009(2)
O(4)	0.2368(4)	0.484(1)	0.4657(5)	0.008(2)

[a] $U_{eq} = 1/3 \sum_i \sum_j (U_{ij} a_i^* a_j^* \mathbf{a}_i \cdot \mathbf{a}_j)$

TABLE 3
Relevant Interatomic Distances (Å) and Angles (°) with ESD's for the $M_2Te_3O_8$ Phases

		M = Co	M = Ni	M = Cu	M = Zn
M–O(1)		2.031(4)	2.013(4)	1.916(4)	2.018(6)
–O(2)		2.174(4)	2.071(5)	1.961(4)	2.197(5)
–O(3)		2.050(4)	2.000(4)	2.174(4)	2.029(5)
–O(3)		2.060(4)	2.054(4)	2.005(4)	2.068(5)
–O(4)		2.132(4)	2.189(3)	2.129(4)	2.116(5)
–O(4)		2.312(4)	2.184(3)	2.782(4)	2.490(5)
Te(1)–O(1)	2×	1.870(4)	1.872(4)	1.874(4)	1.873(6)
–O(2)	2×	2.096(4)	2.101(5)	2.090(4)	2.097(5)
Te(2)–O(2)		1.942(4)	1.962(4)	1.979(4)	1.942(5)
–O(3)		1.875(4)	1.884(4)	1.861(4)	1.859(5)
–O(4)		1.920(4)	1.930(4)	1.928(4)	1.905(5)
–O(4)		2.342(4)	2.322(4)	2.205(4)	2.324(5)
O(1)–Te(1)–O(1)		102.5(3)	101.3(2)	102.1(3)	101.6(4)
O(1)–Te(1)–O(2)	2×	84.2(2)	83.8(2)	82.3(2)	83.8(2)
O(1)–Te(1)–O(2)	2×	90.5(2)	91.0(2)	91.5(2)	91.4(3)
O(2)–Te(1)–O(2)		171.6(3)	171.9(2)	170.3(2)	172.4(3)
O(2)–Te(2)–O(3)		94.1(2)	95.3(2)	92.7(2)	93.1(2)
O(2)–Te(2)–O(4)		81.5(2)	81.3(2)	79.3(2)	81.9(2)
O(2)–Te(2)–O(4)		154.2(2)	155.2(2)	154.1(2)	155.1(2)
O(3)–Te(2)–O(4)		97.1(2)	95.7(2)	97.7(2)	97.3(2)
O(3)–Te(2)–O(4)		81.2(2)	82.0(2)	89.4(2)	83.8(2)
O(4)–Te(2)–O(4)		73.9(2)	74.4(1)	74.8(2)	74.2(2)
O(1)–*M*–O(2)		172.6(2)	173.1(2)	170.9(2)	169.9(2)
O(1)–*M*–O(3)		95.9(2)	93.8(2)	98.0(2)	97.6(2)
O(1)–*M*–O(3)		100.9(2)	97.0(2)	97.3(2)	102.6(2)
O(1)–*M*–O(4)		100.9(2)	100.2(2)	96.3(2)	98.5(2)
O(1)–*M*–O(4)		82.2(2)	83.9(1)	77.6(2)	80.1(2)
O(2)–*M*–O(3)		85.2(2)	86.6(2)	86.7(2)	86.9(2)
O(2)–*M*–O(3)		86.1(2)	89.8(2)	88.8(2)	85.2(2)
O(2)–*M*–O(4)		71.7(2)	73.0(2)	75.0(2)	71.5(2)
O(2)–*M*–O(4)		97.0(1)	95.7(2)	98.3(2)	95.8(2)
O(3)–*M*–O(3)		99.8(1)	97.5(1)	105.0(1)	102.5(1)
O(3)–*M*–O(4)		104.3(2)	102.0(1)	104.4(1)	106.6(2)
O(3)–*M*–O(4)		177.0(2)	177.6(2)	173.8(2)	176.2(2)
O(3)–*M*–O(4)		145.3(1)	153.0(2)	145.4(1)	141.3(2)
O(3)–*M*–O(4)		78.3(1)	81.9(1)	71.6(2)	75.3(2)
O(4)–*M*–O(4)		78.4(2)	79.3(1)	80.6(2)	76.8(2)

temperatures (18). This reaction produces an excessive head pressure, which is evident even when the reaction vessel is frozen in liquid N_2 prior to opening.

Additionally, the nitrates KNO_3, $Ba(NO_3)_2$, and NH_4NO_3 have been used in these reactions in an effort to include the cation in resultant structures. In these cases, the use of reaction conditions similar to those used in chloride mineralizers, particularly the temperature (375°C), could not be used due to the bursting of reaction tubes during heating. By scaling down the reaction temperature to 325°C, which minimized the loss of tubes during heating, it was found that the metal oxide appeared to be too insoluble for reaction. These materials were left as finely divided powders, with the TeO_2 also showing limited recrystallization.

Also, the effect of stoichiometry was examined in an effort to produce other products. In our reaction conditions and relative concentrations (~ 200 mg reaction scale in 0.7 mL of aqueous solution), we have altered the stoichiometry in an effort to produce more metal or more tellurium rich products. In virtually all cases, the primary exception being manganese, these reactions failed to yield different products. Reactions with excess TeO_2 produced the $M_2Te_3O_8$ phase and highly crystalline TeO_2. However, if excess metal oxide was used, the excess would simply be deposited as a mixture with the $M_2Te_3O_8$ compound.

Structural Description

The title phases were shown by single crystal X-ray diffraction to be isostructural to the spiroffite $(Mn, Zn)_2Te_3O_8$ phase. The spiroffite structure is best described in terms of copper tellurium oxide slabs running parallel to the *bc*

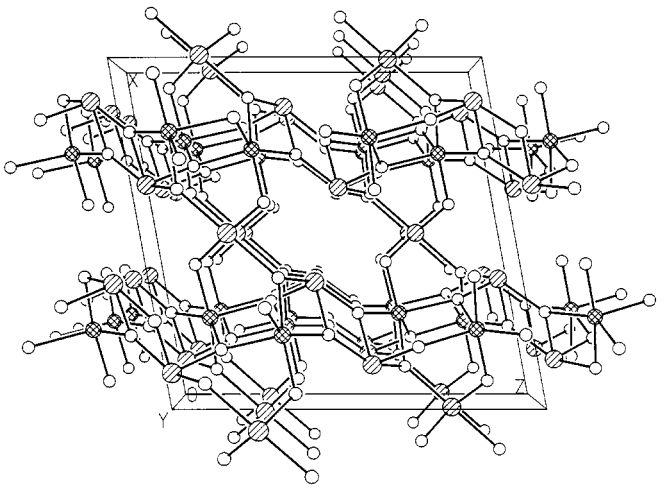

FIG. 1. Unit cell view of $Cu_2Te_3O_8$ shown down the *b* axis. The large, striped circles are tellurium atoms, the cross-hatched circles are copper atoms, and the small, open circles are oxygen atoms.

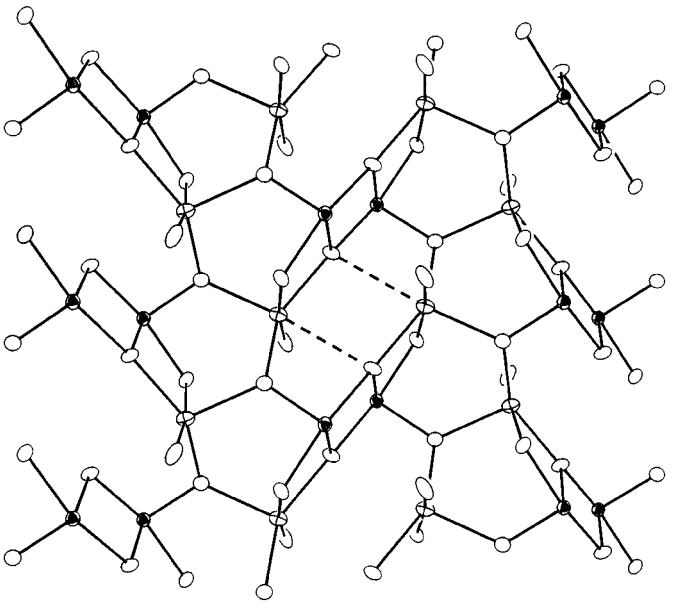

FIG. 2. A view of the copper tellurite slab. The full thermal ellipses are Te(2) atoms, the crossed ellipses are copper atoms, and the boundary ellipses are oxygen atoms. The long sixth distance between copper and oxygen is designated with a dashed bond. All ellipsoids are shown at the 70% probability level.

plane, which are bound to one another by the tellurium atoms (Te(1)) occupying special positions (4e site). A unit cell view of $Cu_2Te_3O_8$ down the *b* axis is shown in Fig. 1. The tellurium atoms within the slab (Te(2)) are all in general positions and are typified by TeO_{3+1} coordination geometry with three Te(2)–O distances ranging from 1.861(5) to 1.980(5) Å and a fourth longer distance of 2.209(5) Å, which compare well with bonding distances in β-$VTeO_4$ of 1.85 to 2.02 Å for the shorter bonds and a longer distance of 2.21 Å (33). In contrast, the tellurium atoms that bind the slabs are in a more regular trigonal bipyramidal TeO_4 environment as constrained by symmetry, with a pair of axial and equatorial Te(1)–O distances of 2.091(5) and 1.873(5) Å, respectively, and O_{ax}–Te(1)–O_{eq} angles of 82.4(2)° and 91.5(2)°. Also, the O_{ax}–Te(1)–O_{ax} angle is 170.3(3)°, which shows a slight distortion due to the presence of a stereochemical lone pair. This overall geometry compares reasonably well with the TeO_4 coordination environment in α-TeO_2, which has Te–O distances of 2.082 and 1.903 Å, and angles of 84.6°, 88.1°, and 168.5° (12).

A view of a fragment of the slab in the *bc* plane is shown in Fig. 2. This slab is made up of Te_2O_6 units, which are generated from the edge-sharing of two TeO_{3+1} pseudotrigonal bipyramids through a pair of oxygen atoms (O(4)). This edge-sharing unit is relatively uncommon, seen in the mineral deningite (Mn, Ca, Zn)Te_2O_5 (34), β-$Li_2Te_2O_5$ (35), β-$VTeO_4$ (33), and $Na_2Te_4O_9$ (36). These Te_2O_6 units are subsequently connected to six other units through pseudooctahedrally coordinated copper atoms. In this pseudooctahedral environment, four oxygen atoms are used primarily to link the copper atoms to the Te_2O_6 units, while one atom is connected exclusively to the linking Te(1)O_4 unit and one is connected to both a Te_2O_6 unit and TeO_4 unit.

In comparing the structural data for the four phases characterized by single crystal X-ray diffraction, the main difference in the structures appears to occur at the transition metal site rather than the tellurite building blocks. In the tellurium sites, the Te(1)–O distances vary, at most, by 0.01 Å from structure to structure, whereas there is a greater degree of variability in the Te(2)–O distances, with the most pronounced differences occurring in the "axial" distances of the TeO_{3+1} unit with respect to the sterochemical lone pair. The distances for these bonds range from 1.941(6) Å in $Zn_2Te_3O_8$ to 1.980(5) Å in $Cu_2Te_3O_8$ for Te(2)–O(2), and 2.209(5) Å in $Cu_2Te_3O_8$ to 2.341(5) Å in $Co_2Te_3O_8$ for Te(2)–O(4). The higher variance in Te(2)–O distances appears to be caused by its proximity to the transition metal in the metal tellurite slabs which make up the structure.

In contrast, the *M*–O distances are highly variable, with differences not only in individual distances but a change in coordination number as well. The copper and zinc compounds each have five definitive bond distances ranging from 1.916(5) to 2.173(5) Å for $Cu_2Te_3O_8$ and 2.011(7) to 2.199(6) Å in $Zn_2Te_3O_8$. There is also a sixth *M*–O distance that is relatively long at 2.783(5) and 2.497(6) Å, for the copper and zinc analogs respectively, which suggests that these metal atoms are essentially five coordinate. In contrast, $Co_2Te_3O_8$ and $Ni_2Te_3O_8$ have six reasonable *M*–O bonding distances ranging from 2.038(5) to 2.312(4) Å and 2.000(4) to 2.185(4) Å, respectively, which would suggest that these two transition metals are six coordinate.

The structure of $Cu_2Te_3O_8$ appears to be the one that is most influenced by its transition metal oxygen environment. As is frequently the case with Cu d^9 compounds, there appears to be a Jahn–Teller distortion in its coordination environment (37). The Cu–O(1) and Cu–O(2) distances, through which the slabs are connected to the linking tellurium atoms, are considerably shorter than those in the remaining three analogs. Furthermore, these two oxygen atoms correspond to the axial sites in the distorted trigonal bipyramidal geometry. There is, in addition to the considerable lengthening of the second Cu–O(4) site, a lengthening of the trans M–O(3) bond in accordance with the Jahn-Teller distortion. These changes result in a lengthening of the a axis and a subsequent shortening of the c axis as compared to the other spiroffite-type compounds.

TABLE 4
Valence Bond Sums for the $M_2Te_3O_8$ Phases[a]

	$Co_2Te_3O_8$	$Ni_2Te_3O_8$	$Cu_2Te_3O_8$	$Zn_2Te_3O_8$
M	1.91(1)	1.907(9)	1.97(1)	1.94(2)
Te(1)	4.13(3)	4.11(3)	4.13(3)	4.07(3)
Te(2)	4.09(3)	4.02(2)	4.04(3)	4.16(3)
O(1)	1.88(2)	1.87(2)	1.85(2)	1.87(2)
O(2)	2.09(2)	2.09(1)	2.20(2)	2.08(2)
O(3)	2.07(2)	2.03(2)	2.04(2)	2.15(2)
O(4)	2.02(2)	2.00(2)	1.98(2)	2.04(2)

[a] $\sum s(M\text{–}L) = \sum \exp[(r_o - r)/0.37]$. s, individual bond valences; r, bond distance in structure; and r_o, empirically derived M–L single-bond distance (Co^{II}–O = 1.692, Ni^{II}–O = 1.654, Cu^{II}–O = 1.679, Zn^{II}–O = 1.704, Te^{IV}–O = 1.977 Å). All distances from table found in Ref. (38).

Bond Valence Sums

The bond valence sums (38) were calculated for the four fully structurally characterized compounds in order to ensure that there were no anomalous results due to the lack of a linear periodic trend in the lattice parameters and M–O environments. For the calculations, oxygen was assigned its common -2 oxidation state and tellurium was assumed to be tetravalent based on the presence of an observed stereochemical lone pair at all sites. Based on these assignments, the oxidation state of the transition metal site is fixed as divalent. As shown in Table 4, there are no significant experimental deviations from the expected values in any of the $M_2Te_3O_8$ compounds.

Physical Characterization

Magnetic susceptibility data were obtained for the cobalt, copper, and nickel analogs of $M_2Te_3O_8$. These phases either were obtained in high purity (Ni) or could be physically separated from their side products in suitable quantities (Co, Cu) for SQUID analysis. The zinc analog was not measured due to difficulties in separating clear crystals from their clear side products, but it is expected to exhibit diamagnetic behavior, due to the closed-shell nature of Zn^{2+}.

The cobalt, nickel, and copper compounds all show Curie–Weiss behavior at higher temperatures and undergo antiferromagnetic transitions with Neel temperatures (T_N) of 35, 70, and 100 K for the nickel, cobalt, and copper analogs, respectively. By using plots of χ^{-1} vs temperature, the linear portion above T_N could be fit to Curie–Weiss behavior. The Curie-Weiss constants, as well as T_N, are shown in Table 5, and a typical temperature dependant plot of χ^{-1} for $Ni_2Te_3O_8$ is shown in Fig. 3.

The experimental moment of the transition metal sites was calculated from the Curie constant. For $Cu_2Te_3O_8$, the moment is 1.90 BM/Cu center, which is slightly higher than the calculated spin only value of 1.73 BM for a Cu(II) atom. This increase is possibly caused by a small angular contribution. The moment for $Ni_2Te_3O_8$ is 3.24 BM/Ni atom, which is also larger than the calculated spin only value of 2.83 BM for a high spin Ni^{2+} ion, but corresponds to observed values for other Ni^{2+} compounds with angular contributions (39). In the cobalt analog, the moment of 5.13 BM/Co atom is also higher than its spin only calculated value of 4.90 BM for high spin Co^{2+}, but is within the range expected for materials with an angular contribution.

Diffuse reflectance spectroscopy was used to determine the optical band gap of the three compounds obtained in high purity. A plot of absorbance vs energy for $Co_2Te_3O_8$ is shown in Fig. 4. In all three compounds, the plots of (absorbance)$^{1/2}$ vs energy at the absorption edge had a better linear dependence than did the plots of (absorbance)^2 vs energy, which suggests that these materials have indirect band gaps (40). Therefore, the band gap for each compound was obtained by determining the inflection point of the first derivative curve of reflectance vs energy. The band gaps were 3.60 eV for $Co_2Te_3O_8$, 3.84 eV for $Ni_2Te_3O_8$, and 2.64 eV for $Cu_2Te_3O_8$.

In addition to the absorption edges, there are lower energy peaks in all three plots, indicative of spin allowed transitions at the metal centers. In the copper analog, there is only one observed transition, which manifests itself as a broad peak at 1.41 eV or 11400 cm^{-1}. This value is in excellent agreement with observed $^2E_{2g} \rightarrow {}^2T_{2g}$ transitions with broadening presumably due to the distortions from

TABLE 5
Neel Temperatures (T_N) and Curie–Weiss Constants for $M_2Te_3O_8$

	T_N (K)	C (emu K/mol)	θ (K)
$Co_2Te_3O_8$	70	6.563	−112
$Ni_2Te_3O_8$	35	2.629	−64
$Cu_2Te_3O_8$	100	0.903	−153

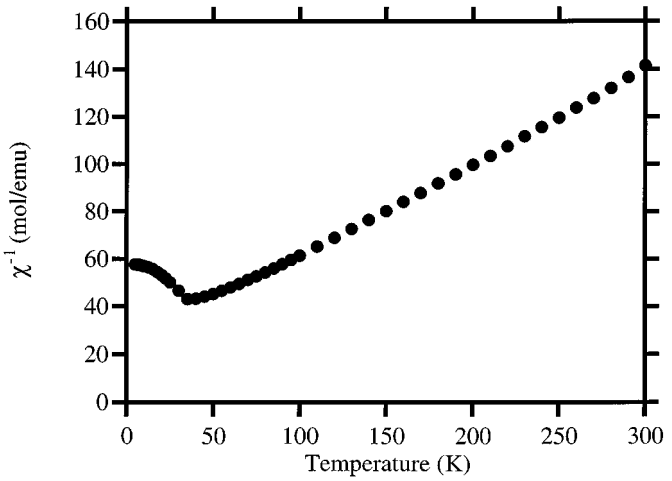

FIG. 3. Plot of inverse magnetic susceptibility (χ^{-1}) vs temperature (K) for $Ni_2Te_3O_8$. The plots of $Cu_2Te_3O_8$ and $Co_2Te_3O_8$ are similar in shape.

ideal octahedral geometry (41). The cobalt and nickel compounds both have three easily discernible transitions, but the nickel compound displays a possible fourth transition in close proximity to one of the peaks. In the cobalt compound, the three transitions occur at 0.95 eV (7700 cm^{-1}), 1.63 eV (13200 cm^{-1}), and 2.23 eV (18000 cm^{-1}). These peaks are very close in value to those expected for $^4T_{1g} \rightarrow {}^4T_{2g}$, $^4T_{1g} \rightarrow {}^4A_{2g}$, and $^4T_{1g} \rightarrow {}^4T_{1g}$ bands (42). However, the $^4T_{1g} \rightarrow {}^4A_{2g}$ band is normally weak and appears unusually strong in our case. In the nickel analog, the transitions are at 0.92 eV (7400 cm^{-1}), a doublet peak with maxima at 1.61 eV (13000 cm^{-1}) and 1.73 eV (13900 cm^{-1}), and 2.81 eV (22600 cm^{-1}). These are exactly what is expected for the spin allowed transitions $^3A_{2g} \rightarrow {}^3T_{2g}$, $^3A_{2g} \rightarrow {}^3T_{1g}$ (F), and $^3A_{2g} \rightarrow {}^3T_{1g}$ (P) (43).

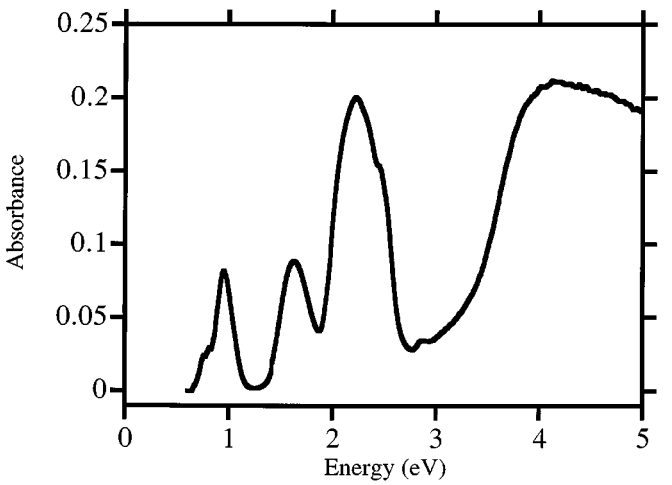

FIG. 4. Diffuse reflectance spectrum for $Co_2Te_3O_8$, showing absorption edge and bands due to allowed transitions at the transition metal center. The spectra for $Cu_2Te_3O_8$ and $Ni_2Te_3O_8$ are similar.

TABLE 6
Lattice Parameters for the $M_2Te_3O_8$ Phases Obtained from Powder Diffraction

Compound	a (Å)	b (Å)	c (Å)	β (°)
$Mn_2Te_3O_8$	12.896(5)	5.398(2)	11.907(5)	98.14(4)
$Co_2Te_3O_8$	12.659(6)	5.205(1)	11.619(4)	99.08(3)
$Ni_2Te_3O_8$	12.388(3)	5.196(1)	11.495(3)	98.74(2)
$Cu_2Te_3O_8$	11.826(4)	5.263(2)	12.230(5)	100.32(3)
$Zn_2Te_3O_8$	12.663(6)	5.191(2)	11.769(4)	99.60(3)

CONCLUSION

Five first row divalent transition metal tellurites with the spiroffite structure ($M_2Te_3O_8$) have been prepared as well-formed single crystals in good yield from hydrothermal solutions. Three of these compounds (M = Co, Ni, Cu) have proven to be wide band gap, antiferromagnetic materials. The remaining two compounds, $Mn_2Te_3O_8$ and $Zn_2Te_3O_8$, could not be fully characterized due to difficulties in physical separation. However, it can be assumed that the colorless, closed shell zinc compound would also be a wide band gap material with a small diamagnetic signal. Although the physical characteristics cannot be approximated without further measurement, the lattice parameters of $Mn_2Te_3O_8$ (Table 6) suggest that the structure of the material will be similar to the cobalt and nickel compounds due to a similar a/c ratio and small β angle.

All attempts to synthesize an iron analog failed, as oxide-based iron sources proved to be unreactive, while using $FeCl_2$ resulted in the formation of $H_3Fe_2(TeO_3)_4Cl$ (28, 30). In all cases, the use of mineralizers other than NH_4Cl failed to yield crystalline products. The spiroffite compounds appear to be highly stable to moisture and air and can be synthesized despite wide ranges of starting stoichiometries. Reactions using higher ratios of metal oxides tended to yield a mixture of metal oxides and the $M_2Te_3O_8$ phase, whereas reactions loaded with excess TeO_2 only deposit the excess as well-faceted clear crystals.

ACKNOWLEDGMENTS

The authors thank Thomas P. Thrash at Rice University for the SQUID measurements. This work was supported by the National Science Foundation under Grant CHE-9102548.

REFERENCES

1. J. E. Stanworth, *Nature* **169,** 582 (1952).
2. H. Burger, W. Vogel, and V. Kozhukharov, *Infrared Phys.* **25,** 395 (1985).
3. K. Tanaka, T. Yoko, H. Yamada, and K. Kamiya, *J. Non-Cryst. Solids* **103,** 250 (1988).
4. V. K. Dhawan, A. Mansingh, and M. Sayer, *J. Non-Cryst. Solids* **51,** 87 (1982).

5. C. R. Feger and J. W. Kolis, *Acta Crystallogr. C* **54,** 1055 (1998).
6. C.R. Feger and J. W. Kolis, *Inorg. Chem.* **37,** 4046 (1998).
7. K. Hanke, V. Kupcik, and O. Lindqvist, *Acta Crystallogr. B* **29,** 963 (1973).
8. F. Pertlik, *J. Solid State Chem.* **71,** 291 (1987).
9. C. Platte and M. Trömel, *Acta Crystallogr. B* **37,** 1276 (1981).
10. W. Abriel, *Z. Naturforsch. B* **36,** 405 (1981).
11. C. R. Feger and J. W. Kolis, *Acta Crystallogr. C* **54,** 1217 (1998).
12. O. Lindqvist, *Acta Chem. Scand.* **22,** 977 (1968).
13. J. A. Mandarino, S. J. Williams, and R. S. Mitchell, *Am. Mineral.* **47,** 196 (1962).
14. K. Hanke, *Naturwissenschaften* **53,** 273 (1966).
15. O. J. Lieder and G. Gattow, *Naturwissenschaften* **56,** 460 (1969).
16. G. Perez, F. Lasserre, J. Moret, and B. Frit, *CR Acad. Sci. Paris., Ser. C* **272,** 77 (1971).
17. M. Trömel and D. Schmid, *Z. Anorg. Allg. Chem.* **387,** 230 (1972).
18. A. Rabenau, *Angew. Chem., Int. Ed. Engl.* **24,** 1026 (1985).
19. L. Falck, O. Lindqvist, and W. Mark, *Acta Crystallogr. B* **34,** 1450 (1978).
20. Card No. 32-0318, JCPDS-ICDD database Joint Commission on Powder Diffraction Standards, International Centre for Diffraction Data, Swarthmore, Pennsylvania, 1991.
21. G. Bayer, *Z. Kristallogr.* **124,** 131 (1967).
22. "TEXSAN: Single Crystal Structure Analysis Software, version 1.6b." Molecular Structure Corp., The Woodlands, Texas, 1993.
23. G. M. Sheldrick, "SHELXTL-Plus," version 4.2, Structure Determination Software Program, Siemens Analytical X-ray Instruments, Inc., Madison, Wisconsin, 1990.
24. A. C. T. North, D. C. Phillips, and F. S. Mathews, *Acta Crystallogr. A* **24,** 351 (1968).
25. A. C. Larson, "Crystallographic Computing" (F. R. Ahmed, S. R. Hall, and C. P. Huber, Eds.) pp. 291–294. Munksgaard, Copenhagen, 1970.
26. Y. LePage, *J. Appl. Crystallogr.* **20,** 264 (1987).
27. A. L. Spek, *Acta Crystallogr. A* **46,** C34 (1990).
28. W. W. Wendlandt and H. G. Hecht, "Reflectance Spectroscopy." Interscience Publishers, New York, 1966.
29. Y. Dusausoy, J. Protas, *Acta Crystallogr. B* **25,** 1551 (1969).
30. R. Astier, E. Philippot, J. Moret, and M. Maurin, *CR Acad. Sci. Paris, Ser. C* **280,** 1141 (1975).
31. C. R. Feger, J. W. Kolis, K. Gorny, and C. Pennington, *J. Solid State Chem.* **143,** 254 (1999).
32. W. M. Latimer, "Oxidation Potentials," 2nd ed., Prentice Hall, New York, 1952.
33. G. Meunier, J. Darriet, and J. Galy, *J. Solid State Chem.* **6,** 67 (1973).
34. E. M. Walitzi, *Naturwissenschaften* **51,** 334 (1964).
35. D. Cachaut-Herrelillat, A. Norbert, M. Maurin, and E. Phillipot, *J. Solid State Chem.* **37,** 352 (1981).
36. S. L. Tagg, J. C. Huffman, and J. W. Zwanziger, *Chem. Mater.* **6,** 1884 (1994).
37. L. Orgel and J. D. Dunitz, *Nature* **179,** 462 (1957).
38. I. D. Brown and D. Altermatt, *Acta Crystallogr. B* **41,** 244 (1985).
39. A. R. West, "Solid State Chemistry and Its Applications." Wiley, New York, 1984.
40. J. I. Pankove, "Optical Processes in Semiconductors." Prentice Hall, Englewood Cliffs, NJ, 1971.
41. J. Bjerrum, C. J. Ballhausen, and C. K. Jorgensen, *Acta Chem. Scand.* **8,** 1275 (1954).
42. S. Koide, *Phil. Mag.* **4,** 243 (1959).
43. C. K. Jorgensen, *Acta Chem. Scand.* **9,** 1362 (1955).